
**Liquid Crystals**
Publication details, including instructions for authors and subscription information:
http://www.informaworld.com/smpp/title~content=t713926090

# Computer simulation of chiral liquid crystal phases VIII. Blue phases of the chiral Gay-Berne fluid

R. Memmer

Online publication date: 06 August 2010

**To cite this Article** Memmer, R.(2000) 'Computer simulation of chiral liquid crystal phases VIII. Blue phases of the chiral Gay-Berne fluid', Liquid Crystals, 27: 4, 533 — 546
**To link to this Article: DOI:** 10.1080/026782900202723
**URL:** http://dx.doi.org/10.1080/026782900202723

LIQUID CRYSTALS, 2000, VOL. 27, NO. 4, 533–546

# Computer simulation of chiral liquid crystal phases VIII. Blue phases of the chiral Gay–Berne fluid†

R. MEMMER

Fachbereich Chemie, Universität Kaiserslautern, D-67663 Kaiserslautern, Germany; e-mail: memmer@rhrk.uni-kl.de

(*Received 2 September 1999; accepted 18 November 1999*)

The phase diagram of chiral calamitic liquid crystals was studied in the temperature–chirality parameter plane by means of computer simulation. Bulk systems composed of $N = 2048$ uniaxial chiral calamitic Gay–Berne molecules, i.e. with interactions described by the Gay–Berne potential and an additive term for the energy of the chiral interaction, were investigated using Monte Carlo (MC) simulations in the canonical ensemble ($NVT$). A rich polymorphism of chiral liquid crystal phases was observed along an isotherm with increasing chirality parameter describing the strength of the chiral interaction. In addition to the cholesteric phase (N*), for the first time a blue phase I (BP I) could be proven by computer simulation of a many-particle system based on model intermolecular interactions. Additionally, at high values of the chirality parameter, a phase with randomly oriented squirming double twist tubes was found as characteristic for the so-called spaghetti model for blue phase III (BP III). The structures of all phases were characterized by order parameters, a set of scalar and pseudoscalar orientational correlation functions, and especially by visual representations of selected configurations.



## 1. Introduction

Liquid crystals are a state of matter with long range orientational order and in some cases also long range positional order. Molecular chirality of the constituent mesogenic molecules leads to a variety of chiral liquid crystal phases [1] which are of interest from the theoretical point of view as well as for their material properties. Characteristic for these phases are helical superstructures in the arrangement of the molecules, i.e. the manifestation of suprastructural chirality [2], based on a spontaneous twist of the molecular orientation. Well known examples for chiral liquid crystal phases without positional order are the cholesteric phase (N*) and the three blue phases (BP I, BP II, and BP III), which are formed by chiral calamitic and discotic molecules in single component systems and induced by chiral dopants dissolved in achiral liquid crystal host phases [1–5]. There exist also many chiral liquid crystal phases with long range positional order, where the formation of both a helical superstructure and a layered structure (a) can be realized free of defects, as for example in SmC* phases of calamitic molecules or columnar phases with helical intracolumnar order of the discotic molecules [6], or (b) yields frustrated structures, as in the case of the recently discovered different twist grain boundary phases (TGB) with a helical arrangement of smectic regions [7] or blue phases with smectic order [8]. In spite of the enormous success in the determination and characterization of new structures of chiral liquid crystal phases, relatively little is known about the connection between the molecular chirality and the suprastructural chirality of the phases, i.e. about the link between chirality at the microscopic and the macroscopic levels, as recently pointed out by Lubensky *et al.* [9]. Only in part is this link understood, e.g. with respect to the helical superstructure of induced cholesteric phases, the surface chirality model of Ferrarini *et al.* [10] allows one to predict both the handedness and the pitch for a given chiral dopant. Especially, the determination of phase diagrams in the temperature–chirality parameter plane and of the structures of the different blue phases has been the subject of many experimental and theoretical investigations even since the discovery of liquid crystals [11–14], but in general it is very difficult to make predictions about the chiral liquid crystal phases or even the phase sequence appearing for a selected chiral mesogenic molecule.

Investigations by means of computer simulation, e.g. the Monte Carlo (MC) and molecular dynamics (MD) methods, allow one to deduce a link between microscopic and macroscopic properties starting with model interactions between the particles [15, 16]. Both methods have a long tradition in the study of structural properties

† Presented at the 17th International Liquid Crystal Conference, 19–24 July 1998, Strasbourg, France.

*Liquid Crystals* ISSN 0267-8292 print/ISSN 1366-5855 online © 2000 Taylor & Francis Ltd
http://www.tandf.co.uk/journals/tf/02678292.html

of liquid crystal phases using a broad range of models from more simplified lattice systems, hard core particles, single site potentials up to atomistic systems [17, 18]. Especially, the phase behaviour of the Gay–Berne fluid, a suitable single site model system for achiral liquid crystalline phases, has been the subject of many recent investigations [19]. The phase diagram has been investigated in detail in terms of its dependence on temperature and pressure, as well as on potential parameters controlling the anisotropy of the attractive and repulsive parts of the interactions. It shows a rich polymorphism of achiral liquid crystal phases, e.g. nematic, smectic A and smectic B phases could be proven in systems of calamitic Gay–Berne molecules. Recently, a variety of model systems for chiral liquid crystal phases has been studied, too. Here, the investigations are more or less restricted to the cholesteric phase, as in the first study of chiral liquid crystal phases considering the Berne–Pechukas potential, taking into account chiral interactions [20], or in studies of systems composed of rigid, chiral Gay–Berne molecules defined by joining the centres of Gay–Berne particles through bonds [21, 22], and of lattice systems of chiral molecules [23–25]. The only model system where a rich polymorphism of chiral liquid crystal phases has been proven is given by the chiral Gay–Berne fluid defined taking into account an additive chiral interaction term [26]. Both for chiral calamitic and discotic molecules it shows a rich polymorphism of chiral liquid crystal phases dependent on a pseudoscalar chirality parameter, as determined by MC simulations. In a bulk system of $N = 256$ chiral calamitic Gay–Berne molecules, in addition to a cholesteric phase, for the first time a blue phase (BP II) and a phase with both a helical superstructure and smectic layers could be localized in the temperature–chirality parameter plane of the phase diagram by computer simulations of a many-particle system [26]. A transition from a cholesteric phase to a blue phase, again BP II, could also be determined in a recent study of systems of $N = 256$ chiral discotic Gay–Berne molecules along an isotherm with increasing chirality parameter [27]. This dominance of BP II, which is characteristic for phase diagrams determined theoretically by means of the Landau–de Gennes theory too (see for example [12, 13]), is in contradiction to many experimentally observed phase diagrams; these often showed remarkably universal features with respect to the appearance of cholesteric and blue phases with typical phase sequences N*–BP I–BP II–BP III–Isotropic both with increasing temperature and increasing chirality parameter [28]. Additionally, it has been observed experimentally that the BP II range is very narrow and always disappears at high values of the chirality parameter [28]. Recently, this latter feature has been obtained for the first time in a theoretically determined phase diagram in the temperature–chirality parameter plane, taking into account the influence of fluctuations which at the same time allow one to characterize BP III as a second isotropic phase in agreement with experimental results [29]. A possible reason for the discovered dominance of BP II in the computer simulation studies of chiral Gay–Berne systems could be given in terms of the small system sizes. In the following account a computer simulation study of the phase structures of chiral calamitic liquid crystals will be presented, investigating enlarged systems of uniaxial chiral calamitic Gay–Berne molecules. Of central interest are the characterization of the structural properties of the phases and the determination of the phase sequence as a function of the strength of the chiral interactions, focusing especially on the formation of blue phases. Here, especially the influence of the system size under investigation will be studied in order to elucidate system size effects with respect to the formation of BP II. Additionally, investigations at high values of the chirality parameter will be performed with respect to the appearance of BP III and with regard to its structure, which is still under discussion.



## 2. Model system

The total intermolecular interaction energy $U(\Omega_i, \Omega_j, \mathbf{r}_{ij})$ between two chiral molecules $i$ and $j$ with orientations denoted by $\Omega_i$ and $\Omega_j$, respectively, separated by an intermolecular vector $\mathbf{r}_{ij}$ can be decomposed into two parts, see e.g. [30], the energy of the achiral interaction $U_a(\Omega_i, \Omega_j, \mathbf{r}_{ij})$ and the energy of the chiral interaction $U_c(\Omega_i, \Omega_j, \mathbf{r}_{ij})$, i.e.

$$U(\Omega_i, \Omega_j, \mathbf{r}_{ij}) = aU_a(\Omega_i, \Omega_j, \mathbf{r}_{ij}) + cU_c(\Omega_i, \Omega_j, \mathbf{r}_{ij}) \tag{1}$$

where $a$ and $c$ have been introduced as dimensionless scalar and pseudoscalar parameters, respectively, measuring the strength of the corresponding interaction energy. The normalized parameter $c^* = c/a$ can be used as a chirality parameter, which changes sign if the interacting chiral molecules are replaced by their mirror images, i.e. by the enantiomers.

For the chiral Gay–Berne fluid [26], the energy of the achiral interaction $U_a(\Omega_i, \Omega_j, \mathbf{r}_{ij})$ between two uniaxial chiral molecules is taken as proposed by Gay and Berne [31] to be

$$U_a(\hat{\mathbf{u}}_i, \hat{\mathbf{u}}_j, \mathbf{r}_{ij}) = \left\{4\varepsilon(\hat{\mathbf{u}}_i, \hat{\mathbf{u}}_j, \hat{\mathbf{r}}_{ij})\left[\left(\frac{\sigma_0}{r_{ij} - \sigma(\hat{\mathbf{u}}_i, \hat{\mathbf{u}}_j, \hat{\mathbf{r}}_{ij}) + \sigma_0}\right)^{12} - \left(\frac{\sigma_0}{r_{ij} - \sigma(\hat{\mathbf{u}}_i, \hat{\mathbf{u}}_j, \hat{\mathbf{r}}_{ij}) + \sigma_0}\right)^{6}\right]\right\} \tag{2}$$

where $\hat{\mathbf{r}}_{ij}$ denotes the unit vector parallel to $\mathbf{r}_{ij}$ and $r_{ij} = |\mathbf{r}_{ij}|$. The orientation is described by the unit vectors $\hat{\mathbf{u}}_i$ and $\hat{\mathbf{u}}_j$ along the symmetry axes of the rotationally symmetric molecules. For positive values of the scalar parameter $a$, an orientation with parallel vectors $\hat{\mathbf{u}}_i$ and $\hat{\mathbf{u}}_j$ as in a nematic phase is energetically preferred, whereas parameterizations of the orientation- and separation-dependent parameters $\sigma(\hat{\mathbf{u}}_i, \hat{\mathbf{u}}_j, \hat{\mathbf{r}}_{ij})$ and $\varepsilon(\hat{\mathbf{u}}_i, \hat{\mathbf{u}}_j, \hat{\mathbf{r}}_{ij})$ can be chosen (see for example [19] for the explicit expressions) suitable for calamitic molecules favouring a side-by-side arrangement and suitable for discotic molecules favouring an end-by-end arrangement.

The energy of the chiral interaction $U_c(\Omega_i, \Omega_j, \mathbf{r}_{ij})$ is given by

$$U_c(\hat{\mathbf{u}}_i, \hat{\mathbf{u}}_j, \mathbf{r}_{ij}) = -\left\{4\varepsilon(\hat{\mathbf{u}}_i, \hat{\mathbf{u}}_j, \hat{\mathbf{r}}_{ij})\left[\frac{\sigma_0}{r_{ij} - \sigma(\hat{\mathbf{u}}_i, \hat{\mathbf{u}}_j, \hat{\mathbf{r}}_{ij}) + \sigma_0}\right]^7 \times [(\hat{\mathbf{u}}_i \times \hat{\mathbf{u}}_j)\ \hat{\mathbf{r}}_{ij}]\,(\hat{\mathbf{u}}_i\ \hat{\mathbf{u}}_j)\right\} \quad (3)$$

i.e. proportional to the first pseudoscalar term $[(\hat{\mathbf{u}}_i \times \hat{\mathbf{u}}_j)\ \hat{\mathbf{r}}_{ij}]\,(\hat{\mathbf{u}}_i\ \hat{\mathbf{u}}_j)$ of the expansion of the intermolecular interaction energy in rotational invariants [30], as obtained by van der Meer *et al.* based on the electric multipole expansion [32] for cylindrically symmetric chiral molecules, in terms also of the orientations of the symmetry axes. The energy of the chiral interaction favours a twisted orientation of the molecules, whereas the twist angle of the most preferred orientation depends on the size of the chirality parameter which vanishes if the molecules are achiral. It discriminates energetically between left- and right-handed arrangements depending on the described enantiomer expressed by the sign of the chirality parameter $c^*$.



## 3. Computational details

The chiral Gay–Berne fluid was studied in a cubic box of length $L$ at constant number of particles $N$, volume $V$ and temperature $T$, i.e. in the canonical ensemble ($NVT$), using the standard Metropolis Monte Carlo technique [15, 16]. Cubic periodic boundary conditions and nearest image summation were applied. Scaled units are used in the following: scaled temperature $T^* = k_B T/\varepsilon_0$, scaled density $\rho^* = N\sigma_0^3/V$, scaled energy $\langle U^* \rangle = \langle U \rangle /\varepsilon_0$, scaled distance $r^* = |\mathbf{r}_{ij}|/\sigma_0$, scaled box length $L^* = L/\sigma_0$ and scaled chirality parameter $c^* = c/a$. All simulations were done at a density $\rho^* = 0.3$, with $a = 1$ applying a spherical cut-off at $r^* = 3.8$. For all chiral Gay–Berne particles a parametrization suitable for calamitic molecules with parameter values $\sigma_e/\sigma_s = 3$, $\varepsilon_e/\varepsilon_s = 0.2$, $\mu = 1$ and $\nu = 2$ were used, as already studied for the Gay–Berne fluid [33] and applied in previous investigations of the chiral Gay–Berne fluid [26]. A trial configuration was generated by a random translation of an arbitrarily chosen molecule, followed by a random rotation about one of the randomly chosen space-fixed axes. A bulk system of $N = 2048$ achiral molecules ($c^* = 0$) was equilibrated at $T^* = 1.5$, i.e. in the nematic temperature range of the Gay–Berne fluid [33], starting from an initial configuration with randomly distributed molecular positions and orientations. Along this isotherm the chirality parameter $c^*$ was increased step by step up to $c^* = 2.0$ with a step size of $\Delta c^* = 0.1$, using the final configuration obtained for lower values of $c^*$ as initial configuration for the subsequent run. For each value of the chirality parameter, an equilibration run of 200 kc (1 kc denotes 1000 cycles, i.e. attempted moves per particle) was followed by a production run of 100 kc. The functions of interest were calculated every ten cycles and averaged over the production run. Additionally, correlation functions were calculated from data taken after every tenth cycle of a subsequent 150 kc production run. At selected values of the chirality parameter, chosen to be $c^* = 0.0$, 0.8, 1.1 and 2.0, representing characteristic phases appearing along the isotherm studied, very long simulation runs in the range from 1000 up to 3000 kc have been performed in order to guarantee that the structures obtained are stable. At $c^* = 1.1$ additionally two independent runs of 3000 kc each have been performed, starting from different initial configurations with randomly distributed molecular positions and orientations, in order to have an additional cross check that the structure obtained at this value in the cascade run with increasing chirality parameter represents the equilibrium structure under the conditions given.

## 4. Order parameters and correlation functions

The second rank order parameter $\langle Q^2_{0,0} \rangle$ was calculated during the production run as described in [26] in order to characterize the long range orientational order. It is defined by

$$\langle Q^2_{0,0} \rangle = \left\langle \frac{1}{2}(3\cos^2\beta - 1) \right\rangle = \frac{1}{2}(3g^*_{3333} - 1) \quad (4)$$

where the brackets denote the ensemble average, given in terms of orientational distribution coefficients

$$g_{ijkl} = \frac{1}{8\pi^2}\int \bar{f}(\Omega) a_{ik}(\Omega) a_{jl}(\Omega)\,\mathrm{d}\Omega. \quad (5)$$

$\Omega$ comprises the Eulerian angles $\alpha, \beta, \gamma$ between the space-fixed $x'_i$ coordinate system and the molecule-fixed $x_i$ coordinate system; $a_{ij}$ are the elements of the orthogonal transformation matrix for the $x'_i$ to the $x_i$ system. $\bar{f}(\Omega)$ denotes the orientational distribution function averaged over the simulation box with respect to its positional dependence. The molecule-fixed $x_3$ axis is chosen parallel to the molecular symmetry axis $\hat{\mathbf{u}}_i$. The

index * indicates the reference to the principal axes of $g_{33kl}$. The eigenvalues are arranged in a way that satisfies the relations

$$|g^*_{3311} - g^*_{3322}| < |g^*_{3311} - g^*_{3333}| \tag{6}$$

and

$$|g^*_{3311} - g^*_{3322}| < |g^*_{3322} - g^*_{3333}|. \tag{7}$$

As pointed out in [26] the order parameter $\langle Q^2_{0,0} \rangle$ is equal to the Saupe order parameter $S^*$ for a homogeneous orientational distribution in the box, e.g. for nematic phases, where the eigenvector corresponding to the eigenvalue $g^*_{3333}$ defines the director $\hat{\mathbf{n}}$. For inhomogeneous phases, e.g. in a cholesteric phase, $\langle Q^2_{0,0} \rangle$ has a different meaning. For instance, if only segments of an integer multiple of one half of the pitch $p$ are considered, it describes the local order of the molecule-fixed $x_3$ axes with respect to the helical axis given by the eigenvector corresponding to the eigenvalue $g^*_{3333}$.

In order to characterize the structural properties of the phases in more detail, averages of a suitable subset of the rotational invariant functions $S_{l_1 l_2 j}(\hat{\mathbf{u}}_i, \hat{\mathbf{u}}_j, \hat{\mathbf{r}}_{ij})$ introduced by Stone [34] were considered. The radial orientational correlation functions, calculated in spherical shells around a molecule, i.e. as a function of the intermolecular separation $r^*$, are denoted by

$$S_{l_1 l_2 j}(r^*) = \langle S_{l_1 l_2 j}(\hat{\mathbf{u}}_i, \hat{\mathbf{u}}_j, \hat{\mathbf{r}}_{ij}) \rangle_{(r^*)_{ij}} \tag{8}$$

where the subscript $(r^*)_{ij}$ denotes the average over all pairs of molecules of a configuration separated by a distance $r^*$.

Explicitly, the scalar (even 'total rank' $l_1 + l_2 + j$) radial orientational correlation functions

$$S_{000}(r^*) = g(r^*) \tag{9}$$

$$S_{220}(r^*) = \frac{1}{2\sqrt{5}} \langle 3(\hat{\mathbf{u}}_i \ \hat{\mathbf{u}}_j)^2 - 1 \rangle_{(r^*)_{ij}} \tag{10}$$

and

$$S_{440}(r^*) = \frac{1}{24} \langle 3 - 30(\hat{\mathbf{u}}_i \ \hat{\mathbf{u}}_j)^2 + 35(\hat{\mathbf{u}}_i \ \hat{\mathbf{u}}_j)^4 \rangle_{(r^*)_{ij}} \tag{11}$$

and, in order to characterize helical superstructures, the pseudoscalar (odd 'total rank' $l_1 + l_2 + j$) radial orientational correlation functions

$$S_{221}(r^*) = -\sqrt{\frac{3}{10}} \langle [(\hat{\mathbf{u}}_i \times \hat{\mathbf{u}}_j) \ \hat{\mathbf{r}}_{ij}] (\hat{\mathbf{u}}_i \ \hat{\mathbf{u}}_j) \rangle_{(r^*)_{ij}} \tag{12}$$

and

$$S_{441}(r^*) = \frac{\sqrt{5}}{12} \langle [(\hat{\mathbf{u}}_i \times \hat{\mathbf{u}}_j) \ \hat{\mathbf{r}}_{ij}] [3(\hat{\mathbf{u}}_i \ \hat{\mathbf{u}}_j) - 7(\hat{\mathbf{u}}_i \ \hat{\mathbf{u}}_j)^3] \rangle_{(r^*)_{ij}} \tag{13}$$

were calculated.

Additionally, corresponding longitudinal orientational correlation functions

$$S_{l_1 l_2 j}(r^*_\parallel / d) = \langle S_{l_1 l_2 j}(\hat{\mathbf{u}}_i, \hat{\mathbf{u}}_j, \hat{\mathbf{r}}_\parallel) \rangle_{(r^*_\parallel / d)_{ij}} \tag{14}$$

were calculated, here defined as a function of the intermolecular separation $r^*_\parallel$ along a suitably chosen space-fixed reference axis $\mathbf{r}_\parallel$, with a unit vector denoted by $\hat{\mathbf{r}}_\parallel$, additionally scaled by a selected distance $d$ related to the periodicity of the phase studied. The subscript $(r^*_\parallel / d)_{ij}$ denotes the average over pairs of molecules of a configuration separated by a distance $r^*_\parallel / d$ along the reference axis. This axis has been chosen parallel to the helical axis in cholesteric phases with $d$ taken as the pitch $p$, and along the $\langle 1\,0\,0 \rangle$, $\langle 0\,1\,0 \rangle$ or $\langle 0\,0\,1 \rangle$ directions in blue phases I and II with $d$ taken as half of the lattice constant of the cubic unit cell, respectively.

## 5. Results and discussion

In order to investigate the influence of chirality on the structure of liquid crystalline phases of chiral calamitic molecules, the phase diagram in the temperature–chirality parameter plane of the chiral Gay–Berne fluid was studied as a function of the chirality parameter $c^*$ along the isotherm at temperature $T^* = 1.5$, i.e. in the stability range of the nematic phase (N) of the Gay–Berne fluid [33]. The second rank order parameter $\langle Q^2_{0,0} \rangle$ along the isotherm is given in figure 1 as a function of the chirality parameter $c^*$. Its discontinuities allow the approximate localization of the phase transitions that are appearing and a first characterization of the different phases. A first phase transition is obvious in the region $0.5 < c^* < 0.6$. For lower values of $c^*$ the observed positive values of the order parameters $\langle Q^2_{0,0} \rangle = S^* \approx 0.8$ indicate a favoured orientation of the unit vectors $\hat{\mathbf{u}}_i$

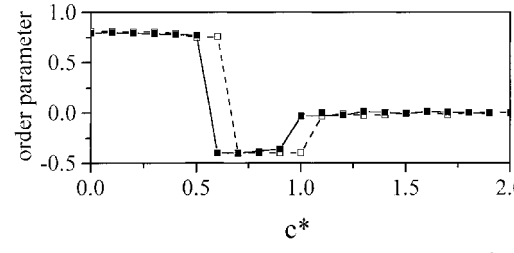


Figure 1. The second rank order parameter $\langle Q^2_{0,0} \rangle$ in a bulk system of $N = 2048$ (■) molecules as a function of the chirality parameter $c^*$ along the isotherm $T^* = 1.5$. Additionally, the values of $\langle Q^2_{0,0} \rangle$ obtained in a system of $N = 256$ (□) molecules are given for comparison [26].

parallel to the space-fixed axis, the director, selected by the algorithm introduced in [26]. The formation of nematic phases, well known at the selected temperature and $c^* = 0.0$ [33], is now maintained until a threshold value of the chirality parameter is reached. For values of the chirality parameter in the range $0.6 \leqslant c^* \leqslant 0.9$ values of $\langle Q^2_{0,0} \rangle \approx -0.42$ indicate a favoured orientation of the unit vectors $\hat{\mathbf{u}}_i$ perpendicular to the selected space-fixed axis, i.e. a behaviour typical in a cholesteric phase with respect to the helical axis. Finally, for higher chirality parameters $c^*$ values of $\langle Q^2_{0,0} \rangle \approx 0.00$ are obtained, indicating an isotropic character of the phase. These findings are in agreement with the phase sequence nematic, cholesteric and blue phases, as already observed in a previous study of a system of $N = 256$ chiral calamitic Gay–Berne molecules [26]. For comparison, the order parameters $\langle Q^2_{0,0} \rangle$ obtained in these smaller systems along the same isotherm are also shown in figure 1 which indicates a system size-dependent stability range of the cholesteric phase. Both the transition from the nematic to the cholesteric and from the cholesteric to the blue phase already appeared in the larger system at smaller values of the chirality parameter. Significant differences are obvious comparing the scaled energy $\langle U^* \rangle$ obtained at different system sizes, shown as a function of the chirality parameter $c^*$ in figure 2. Both at values of the chirality parameter where already $\langle Q^2_{0,0} \rangle$ indicates different phases as a function of the system size (e.g. at $c^* = 0.6$ a cholesteric phase with $N = 2048$ and a nematic phase with $N = 256$ or at $c^* = 1.0$ already a blue phase with $N = 2048$ and still a cholesteric phase with $N = 256$), but also in the interval $0.7 \leqslant c^* \leqslant 0.9$ where a cholesteric phase has been obtained independent of system sizes, the scaled energy $\langle U^* \rangle$ is always significantly lower in the larger system. In the latter case, the more favoured energy indicates that the system size studied enabled the formation of cholesteric phases with values of the pitch $p$ closer to the equilibrium pitch $p_0$.

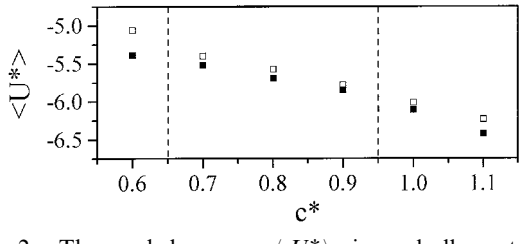


Figure 2. The scaled energy $\langle U^* \rangle$ in a bulk system of $N = 2048$ (■) molecules as a function of the chirality parameter $c^*$ along the isotherm $T^* = 1.5$. Additionally, the values of $\langle U^* \rangle$ obtained in a system of $N = 256$ (□) molecules are given for comparison [26]. The dashed lines form the boundaries of the range of the chirality parameter, where independent of system size cholesteric phases have been formed.

Even more significant is the difference in the scaled energy at $c^* = 1.1$, where independent of the system size, a phase with an isotropic character has been obtained; this will be identified in the following as blue phase I in the system with $N = 2048$ in comparison with the blue phase II identified in the system with $N = 256$ [26].

Visual representations of final configurations from the production runs often allow a characterization of the phases in a simple way. In order to have a schematic representation of its general shape, each molecule is represented in all subsequent snapshots by a rotational symmetric ellipsoid with an axis ratio of 1 : 1 : 3, corresponding to the parameter value $\sigma_e/\sigma_s = 3$, colour coded with respect to the angle between its molecular symmetry axis $\hat{\mathbf{u}}_i$ and a selected space-fixed axis. The characteristics of a cholesteric phase (N*) are obvious in the snapshot of the configuration obtained at the chirality parameter $c^* = 0.8$ shown in figure 3 as representative for values of the chirality parameter in the interval $0.6 \leqslant c^* \leqslant 0.9$ characterized by negative values of $\langle Q^2_{0,0} \rangle$. The configuration is visualized in a view with an in-plane oriented helical axis, which has been formed along a selected diagonal face of the cubic simulation box. The angle between the molecular symmetry axis $\hat{\mathbf{u}}_i$ and the box normal pointing out of plane, i.e. an axis perpendicular

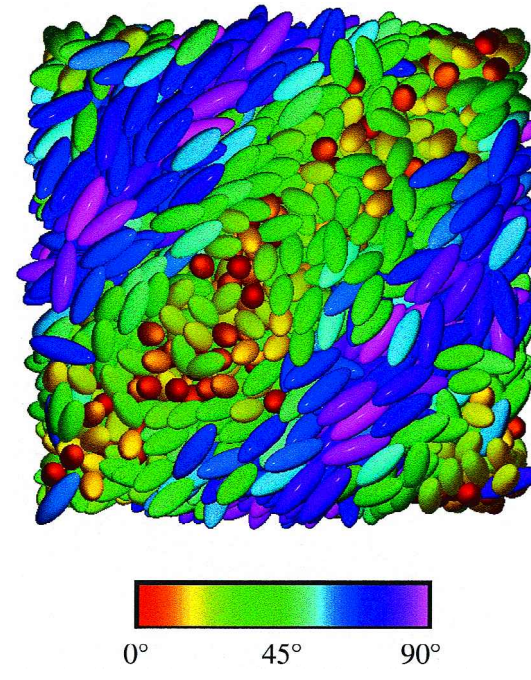


Figure 3. Visualization of a configuration of the cholesteric phase (N*) at chirality parameter $c^* = 0.8$ with an in-plane oriented helical axis. Each molecule is represented by a rotational symmetric ellipsoid with an axis ratio of 1 : 1 : 3 and colour coded with respect to the angle between its unit vector $\hat{\mathbf{u}}_i$ and the out of plane, i.e. perpendicular to the helical axis, oriented box face normal.

to the helical axis, is colour coded. A continuous rotation of the favoured orientation of the molecular axes $\hat{\mathbf{u}}_i$ along the helical axis is obvious, whereas a segment of a cholesteric phase with pitch length $p = \sqrt{2}L$ has been formed. As discussed in detail in [21], under periodic boundary conditions an integral number of half turns of a cholesteric phase has to fit into the simulation box in order to be commensurate with the periodic images, a confinement which in general causes a cholesteric phase with pitch values different from the equilibrium pitch $p_0$ and a threshold value of the chirality parameter necessary for the formation of a cholesteric phase. Experimentally, in systems of chiral only mesogenic molecules with long range orientational order, untwisted structures are stable only under the influence of additional external forces, e.g. applied electric or magnetic fields or induced by surface effects [35]. The situation in canonical simulations using periodic boundary conditions corresponds closely to the experimental situation in a wedge-shaped Cano cell with rigid boundary conditions and parallel orientation at the boundary [35]. In the simulation, for small values of $c^*$ below a threshold value a nematic phase of chiral molecules was favoured. Analogously in the Cano wedge for distances below a critical distance no helical structure can be realized and the system is in a completely untwisted state. In the Cano cell above the threshold value the pitch is a function of the distance $d$ between the two surfaces, and undisturbed helical structures are surrounded by regions with compressed or stretched helical structures. In the simulation the pitch is restricted to values

$$p = \frac{L}{(n_1^2 + n_2^2 + n_3^2)^{1/2}}, n_i = 0, \pm\frac{1}{2}, \pm 1, \pm\frac{3}{2}, \ldots i = 1, 2, 3 \tag{15}$$

where $L$ denotes the box size, i.e. the pitch depends on the system size under investigation. The direction of the helical axis in the space-fixed coordinate system was found to be dominated by the director orientation of the nematic phase used as starting configuration. In the current study, the nematic director was oriented along a diagonal face of the simulation box, which seems to be influenced by boundary effects [36]. In the cholesteric phase, the helical superstructure is preferably formed along an axis perpendicular to the director of the former nematic phase. In principle, other orientations of the helical axis with the same pitch, or even a different pitch constrained according to equation (15), should be possible, but such states are separated by large free energy barriers which make transitions between them rare events. The threshold value shows that, especially in small system sizes at low chirality parameters, a nematic phase, i.e. an untwisted state, is more stable than a cholesteric phase having a necessarily small pitch, i.e. a highly twisted state. The existence of a threshold value in the computer simulation, caused only by boundary effects and not comparable for example to the experimentally proven threshold with respect to the concentration of chiral dopants necessary for the induction of SmC* phases [37], corresponds to the high chiral energy contribution; this is enabled only by relatively high values of the chirality parameter, as a precondition for the stabilization of a cholesteric phase in a system of small size. This explanation is further confirmed by the discovered shift of the threshold value to smaller values in the study of $N = 2048$ molecules, compared with the system of $N = 256$ molecules. Additionally, there are hints for vanishing of the threshold value from an attempt to overcome the above mentioned restrictions using Monte Carlo simulations in the isobaric–isothermal ensemble ($NpT$) [38], where the ability of the simulation box to change dimensions during the simulations should enable the determination of the equilibrium pitch in the cholesteric phase of the chiral Gay–Berne fluid as a function of temperature and chirality parameter.

With increasing chirality parameter, a dramatic change of the structural properties appears, as is obvious in the snapshot of the configuration taken from the production run at $c^* = 1.1$ (figure 4). In spite of order parameters

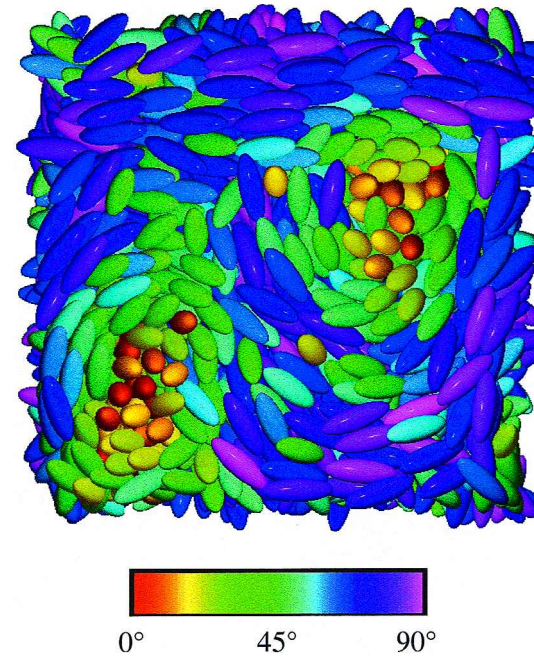


Figure 4. Visualization of a configuration of BP I at chirality parameter $c^* = 1.1$. Each molecule is represented by a rotational symmetric ellipsoid with an axis ratio of 1 : 1 : 3 and colour coded with respect to the angle between its molecular symmetry axis $\hat{\mathbf{u}}_i$ and the out of plane oriented box normal.

$\langle Q^2_{0,0} \rangle$ (figure 1) of zero, regions which show orientational correlations are obvious, especially if the angle between the unit vectors $\hat{\mathbf{u}}_i$ and the box face normal is colour coded. There exist regions where the molecules are preferably parallel to the box face normal, whereas the preferred molecular orientation twists along all directions perpendicular to this axis moving away from these regions, i.e. helical superstructures appear, but only locally and limited about a selected distance. It should be remarked that views on each different box face of the simulation box give the same impression, documenting the equivalence of the structural properties along three orthogonal directions characteristic for cubic blue phases.

The essential parts in the theories of blue phases, which for many chiral mesogens often appear in the sequence BP I–BP II–BP III both with increasing temperature and increasing chirality parameter (see figure 5(*a*) for a schematic phase diagram in the temperature–chirality parameter plane of the phase diagram), are so-called double twist cylinders characterized by a director field as sketched in figure 5(*b*), brought into discussion by Saupe as early as 1969 [39]. Whereas in the cholesteric phase the twisting occurs only in one direction, i.e. along the helical axis, in a double twist cylinder a helical superstructure exists over a selected distance from the cylinder centre along every axis perpendicular to the cylinder axis. Experimentally, such structural elements, whose relevance has been described by de Gennes and Proust [40] with the words 'It thus seems correct that the "double twist" tendency is an essential ingredient of the blue phase. We do not know, however, how close to real life these proposed structures are.', have only been observed in blue phases of lyotropic systems using freeze-fracture electron microscopy [41]. The chiral Gay–Berne fluid is the only many-particle system based on intermolecular interactions where such double twist structures have been proved by computer simulation until now.



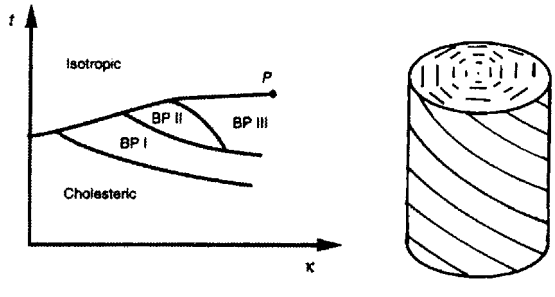


(a) (b)

Figure 5. (*a*) Schematic phase diagram in the temperature–chirality parameter plane (figure from [42]), (*b*) director field of a double twist cylinder (figure from [43]).

Different arrangements of double twist cylinders taking into account unavoidable defects and isotropic regions have been considered as models for blue phases in the framework of Landau–de Gennes theory (see for example [12, 13]), which have been summarized in figure 6. The network of interwoven double twist cylinders in a body-centred cubic structure with space group $O^8$ ($I4_132$), consistent with experimental results for BP I, is shown in figure 6(*a*) as an elementary cell and additionally in figure 6(*b*) in the form of the resulting periodic structure, for the arrangement denoted as the $O^{8-}$ structure in [12]. Characteristic are the infinite double twist cylinders arranged orthogonal to each other, whereas the director on the surface is twisted away 45° from the centre which enables a defect-free director field in regions where two double twist cylinders touch each other.

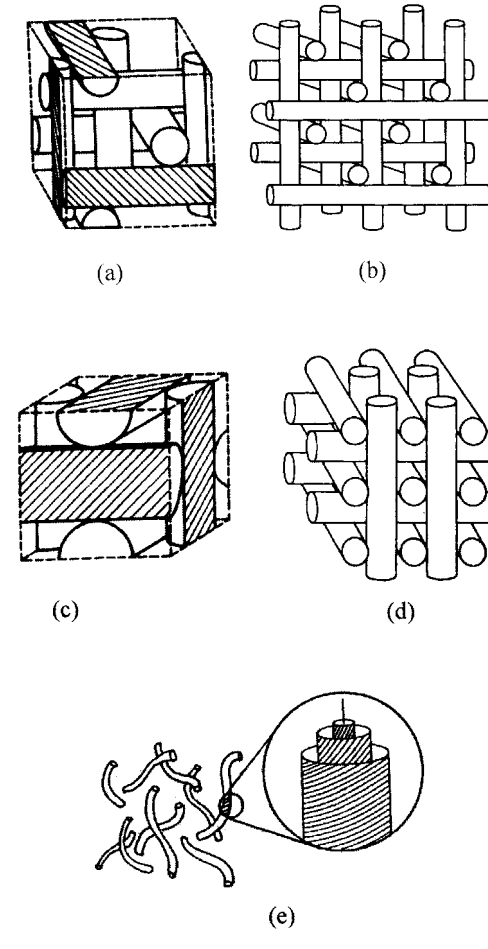

(a) (b) (c) (d) (e)

Figure 6. Theoretical blue phase models: (*a*) BP I, arrangement of double twist cylinders in the unit cell (space group $I4_132$ ($O^8$)); (*b*) BP I, three-dimensional arrangement; (*c*) BP II, arrangement of double twist cylinders in the unit cell (space group $P4_232$ ($O^2$)); (*d*) BP II, three-dimensional arrangement; (*e*) BP III, so-called spaghetti or double twist model with randomly oriented squirming double twist tubes (figures from [8, 12, 44]).

In order to yield a better impression of the arrangement of the several double twist cylinders visible in the configuration taken from the production run at $c^* = 1.1$ (figure 4), and for a better comparison with the theoretical model, in figure 7 the snapshot additionally surrounded by identical images as given by the periodic boundary conditions is shown. It presents two parallel intersections taken perpendicular to the selected out of plane oriented box normal, taken as the $z$ axis, at $z^* = L^*$ and $z^* = 3L^*14$, where $L^*$ denotes the scaled box length $L$. In agreement with the BP I model, figure 6(*a*), the cylinders normal to the intersection plane are at the same positions in both intersections, i.e. infinite in the limitations of the studied system size, and alternating in position due to the required symmetry. Inside the central simulation box, which corresponds to a unit cell of BP I, i.e. the lattice constant is equal to the box length $L$, six isolated double twist cylinders have been formed spontaneously, two along each of the three orthogonal box face normals which define the $\langle 1\,0\,0 \rangle$, $\langle 0\,1\,0 \rangle$ and $\langle 0\,0\,1 \rangle$ directions. Significant especially are the double twist cylinders oriented perpendicular to those already described, either horizontally (figure 7, above) or vertically oriented (figure 7, below) in the intersections shown, separated by a distance of $L^*14$ along the $z$ axis. According to the fourfold screw axis with a translation vector of a quarter of the lattice constant as characteristic for BP I, these appear again in further intersections, horizontally oriented at $z^* = L^*12$ and vertically oriented at $z^* = L^*14$, but translated by a distance $L^*14$ along the vertically oriented $y$ axis and the horizontally oriented $x$ axis, respectively. In order to have an independent cross check that the BP I structure corresponds to the equilibrium structure under the simulation conditions given, additionally two independent runs of 3000 kc each have been performed at the same value of the chirality parameter ($c^* = 1.1$), starting from different initial configurations with randomly distributed molecular positions and orientations, instead of increasing the chirality parameter starting from a cholesteric phase; both resulted again in the formation of a blue phase I structure remaining stable over these very long simulation runs.

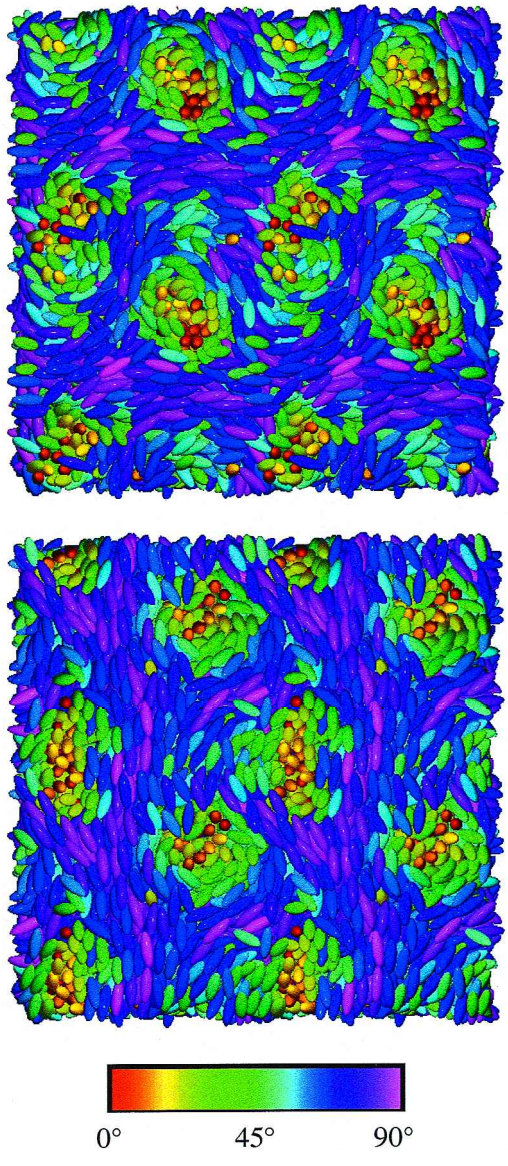


Figure 7. Visualization of a configuration of BP I at chirality parameter $c^* = 1.1$ (snapshot shown in figure 4) surrounded by identical images as given by periodic boundary conditions. Each molecule is represented by a rotational symmetric ellipsoid with an axis ratio of 1 : 1 : 3 and colour coded with respect to the angle between its molecular symmetry axis $\hat{\mathbf{u}}_i$ and the out of plane oriented box face normal. Views on two parallel intersections perpendicular to the out of plane oriented box face normal, separated by a distance of $L^*/4$, are shown.

The influence of the chosen periodic boundary conditions is indicated by the identity of the direction of the box face normals with the $\langle 1\,0\,0 \rangle$, $\langle 0\,1\,0 \rangle$ and $\langle 0\,0\,1 \rangle$ directions, respectively, and by a system size effect with respect to the structure of the blue phases that are appearing. In the system of $N = 256$ molecules at $c^* = 1.1$, a unit cell of a blue phase, shown in figure 8, has also been formed [26], but with a network of interwoven double twist cylinders in a simple cubic structure with space group $O^2$ ($P4_232$), consistent with experimental results for BP II (see for comparison the theoretical BP II model [12, 13] shown in figure 6(*c*) in the form of the elementary cell and in figure 6(*d*) in the form of the resulting periodic structure).

With $N = 256$ the simulation cell was comparably small, so only three isolated double twist cylinders have been formed, one along each of the three orthogonal box face normals, arranged to form a unit cell of BP II. The phase transition discovered from a cholesteric to a BP II [26] was in contradiction to many experimental

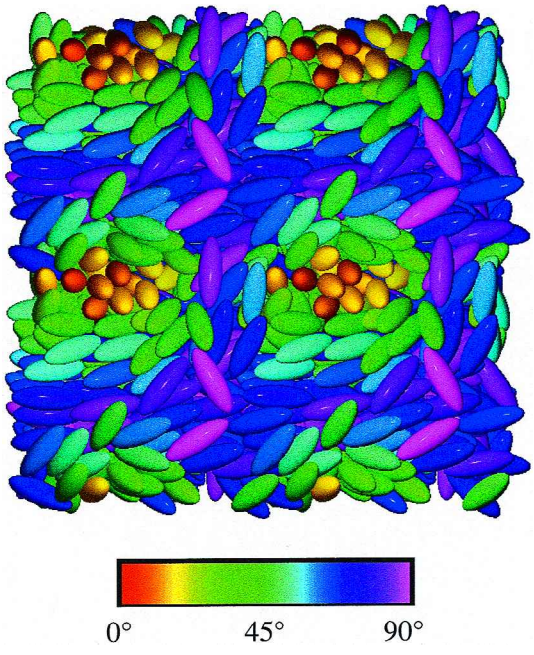


Figure 8. Visualization of a configuration of BP II in a bulk system of $N = 256$ molecules at chirality parameter $c^* = 1.1$ surrounded by identical images as given by periodic boundary conditions [26]. Each molecule is represented by a rotational symmetric ellipsoid with an axis ratio of 1 : 1 : 3 and colour coded with respect to the angle between its molecular symmetry axis $\hat{\mathbf{u}}_i$ and the out of plane oriented box face normal.



results [28]. In the system with $N = 2048$ molecules studied now, in principle eight unit cells of BP II with the lattice constant obtained in [26] could be formed. Energetically more favoured (see figure 2) was the formation of BP I with a doubled lattice constant in this enlarged system, but still with a system size far away from a realistic number of molecules in a unit cell of a blue phase of about $10^7$–$10^8$ [40]. Now, in agreement with the universal phase sequence in the temperature–chirality parameter plane, as sketched in figure 5(*a*), a phase transition from a cholesteric to a blue phase I appeared with increasing chirality parameter along an isotherm. With further increasing chirality parameter, no blue phase II could be observed in the system with $N = 2048$ molecules along the selected isotherm. At the high chirality parameter of $c^* = 2.0$, there still exist local double twist regions, but these are no longer infinite under the limitations of the system size nor arranged in a lattice. In figure 9 two parallel intersections taken perpendicular to the selected out of plane oriented box normal at $z^* = L^*$ and $z^* = L^*12$ of a snapshot are shown. The double twist regions are now worm-like and seem to be randomly oriented as in the so-called spaghetti or double twist model of blue phase III [45], as sketched in figure 6(*e*), which is in addition to the

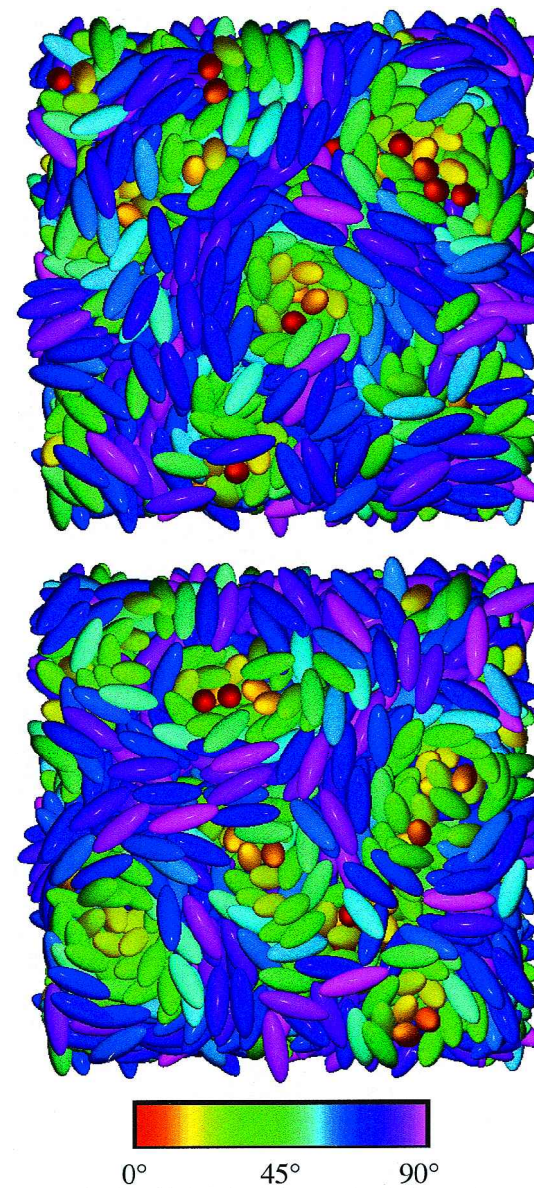


Figure 9. Visualization of a configuration of the phase at chirality parameter $c^* = 2.0$. Each molecule is represented by a rotational symmetric ellipsoid with an axis ratio of 1 : 1 : 3 and colour coded with respect to the angle between its molecular symmetry axis $\hat{\mathbf{u}}_i$ and the out of plane oriented box normal. Views on two parallel intersections perpendicular to the out of plane oriented box face normal, separated by a distance of $L^*/2$, are shown.

icosahedral model and models of bond orientational order [46, 47] still under discussion as a possible structure of BP III.

In order to elucidate the structural features of the phases obtained based on their dependence on the chirality parameter along the selected isotherm, nematic at $c^* = 0.0$, cholesteric at $c^* = 0.8$, blue phase I at $c^* = 1.1$ and the phase with randomly oriented squirming double

twist tubes at $c^* = 2.0$, characterized until now by order parameters and visual representations, several correlation functions were calculated. The distribution of particle centres as a function of the intermolecular separation $r^*$ is shown by the radial distribution function $S_{000}(r^*)$ (figure 10). In the nematic phase $S_{000}(r^*)$ shows the known features at short distances up to $r^* \approx 3.5$, but is structureless for large separations, indicating an isotropic distribution of the molecular centres. With increasing chirality parameter, the near range positional order is enlarged, but the absence of long range positional order is maintained for all values of the chirality parameter studied, i.e. a result in agreement with the experimentally determined properties in cholesteric and blue phases.

The observed phase transitions are accompanied by a change of the orientational order, as already expressed by the behaviour of the order parameter $\langle Q^2_{0,0} \rangle$ (figure 1). Significant differences between the four phases are obvious considering the radial orientational pair correlation function of rank two $S_{220}(r^*)$, figure 11 (*a*), and of rank four $S_{440}(r^*)$, figure 11 (*b*). At short distances, all functions show a maximum with positive values, i.e. the existence of a preferred parallel orientation of the $\hat{\mathbf{u}}_i$ axes of neighbouring molecules which is less extended with increasing chirality parameter. In the nematic phase both $S_{220}(r^*)$ and $S_{440}(r^*)$ rapidly reach a plateau value which is constant over the range of intermolecular separation studied, showing the existence of long range orientational order. On the contrary, both orientational pair correlation functions tend to zero with increasing intermolecular separation in the cholesteric phase and in the blue phases, the latter case starting at shorter distances.

In addition to these scalar orientational correlation functions, a set of pseudoscalar orientational correlation functions was calculated in order to study chiral

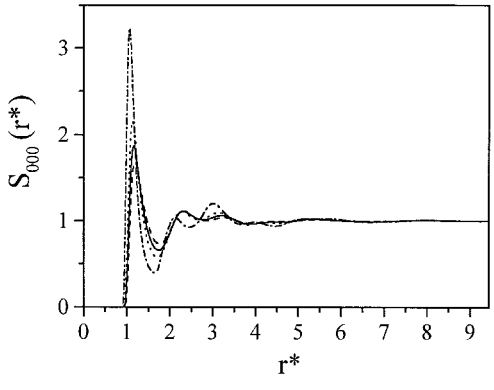


Figure 10. The radial distribution functions $S_{000}(r^*)$ as functions of the intermolecular separation $r^*$ at different values of the chirality parameter $c^*$: in the nematic phase ($c^* = 0.0$, - - -), in the cholesteric phase ($c^* = 0.8$, —), in the BP I ($c^* = 1.1$, . . . ) and in the phase at $c^* = 2.0$ (-. -. -. ).

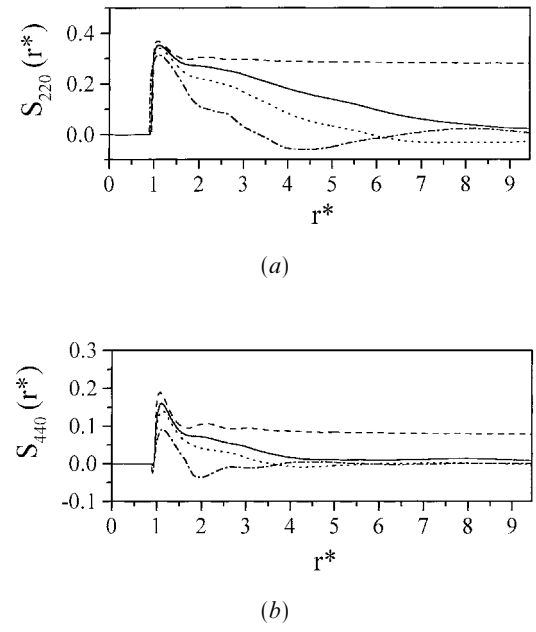


Figure 11. The radial orientational pair correlation functions $S_{220}(r^*)$ (*a*) and $S_{440}(r^*)$ (*b*) as functions of the intermolecular separation $r^*$ at different values of the chirality parameter $c^*$: in the nematic phase ($c^* = 0.0$, - - -), in the cholesteric phase ($c^* = 0.8$, —), in the BP I ($c^* = 1.1$, . . . ) and in the phase at $c^* = 2.0$ (-. -. -. ).

correlations between the molecular orientations and to prove the existence of helical superstructures. The values of the pseudoscalar radial orientational pair correlation functions $S_{221}(r^*)$, figure 12 (*a*), and $S_{441}(r^*)$, figure 12 (*b*), which in the nematic phase are found to be zero for all distances (as it should be in systems where left- and right-handed arrangements have an equal probability), are in all other phases significantly non-zero at short separations, identifying chiral correlations. Both in the cholesteric phase, and even more in the blue phases, the molecules adopt at near range a preferred right-handed orientation indicated by negative values of $S_{221}(r^*)$ and $S_{441}(r^*)$, a handedness determined by the chosen sign of the chirality parameter defining the intermolecular interactions, whereas both functions go to zero for larger distances, $S_{441}(r^*)$ at smaller values of $r^*$.

Especially, in order to understand differences in the different blue phases, selected longitudinal orientational correlation functions have been introduced, which measure correlations as a function of a scaled intermolecular separation $r^*_{\parallel}$ along a suitably chosen reference axis $\mathbf{r}_{\parallel}$, additionally scaled by a selected distance $d$ related to the periodicity of the phase studied. In the cholesteric phase the reference axis has been chosen parallel to the helical axis and $d$ is taken as the pitch $p$. At $c^* = 0.8$ the longitudinal orientational pair correlation function $S_{220}(r^*_{\parallel}/d)$ is modulated corresponding to the periodicity of the orientational correlations along the helical axis in

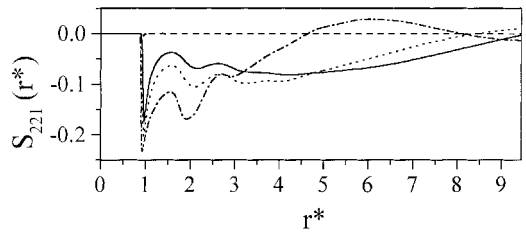


(*a*)

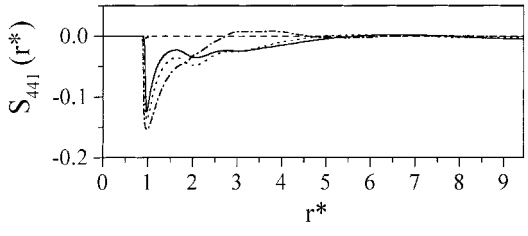


(*b*)

Figure 12. The pseudoscalar radial orientational pair correlation functions $S_{221}(r^*)$ (*a*) and $S_{441}(r^*)$ (*b*) as functions of the intermolecular separation $r^*$ at different values of the chirality parameter $c^*$: in the nematic phase ($c^* = 0.0$, ---), in the cholesteric phase ($c^* = 0.8$, —), in the BP I ($c^* = 1.1$, . . . ) and in the phase at $c^* = 2.0$ (-. -. -. ).

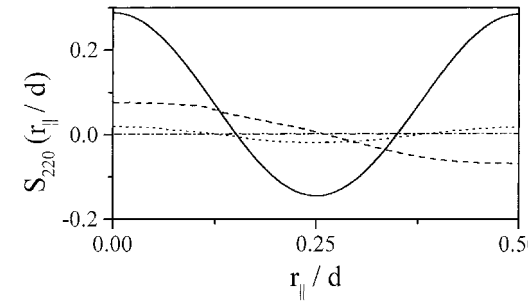


(*a*)

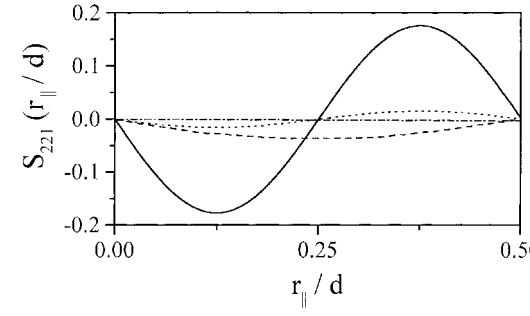


(*b*)

Figure 13. The scalar longitudinal orientational pair correlation functions $S_{220}(r_\parallel^*/d)$ (*a*) and the pseudoscalar longitudinal orientational pair correlation functions $S_{221}(r_\parallel^*/d)$ (*b*) as functions of the intermolecular separation $r_\parallel^*$, scaled by a selected distance $d$ related to the periodicity of the phase studied, at different values of the chirality parameter $c^*$. In the cholesteric phase ($c^* = 0.8$, —) $r_\parallel^*$ denotes the distance in a direction parallel to the helical axis with $d$ taken as the pitch $p$. In the BP I ($c^* = 1.1$, . . . ) and in the phase at $c^* = 2.0$ (-. -. -. ) $r_\parallel^*$ denotes an axis parallel to the normal vector of a selected box face with $d$ taken as half of the box size $L$; for BP I this corresponds to one of the $\langle 1\,0\,0 \rangle$, $\langle 0\,1\,0 \rangle$ and $\langle 0\,0\,1 \rangle$ directions and the lattice constant of the cubic unit cell, respectively. Additionally shown is $S_{220}(r_\parallel^*/d)$ calculated in a BP II (---), obtained in a system of $N = 256$ molecules at $c^* = 1.1$ [26], referenced and scaled as in BP I.

a cholesteric phase, figure 13 (*a*). It varies monotonously from its positive maximum value for molecules separated by small values of $r_\parallel^*/d$ (i.e. here the molecules are preferentially parallel to each other), to its negative minimum value for molecules separated by a distance $r_\parallel^*/d = 1/4$. The molecules separated by this distance are preferentially perpendicular to each other, characterizing this separation as equal to a quarter of the pitch of a cholesteric phase. For larger distances $S_{220}(r_\parallel^*/d)$ increases again until the positive maximum value at $r_\parallel^*/d = 1/2$ is reached, which is in agreement with the periodicity of the cholesteric phase given by half of the pitch. A similar behaviour is obvious in blue phase I at $c^* = 1.1$, where $S_{220}(r_\parallel^*/d)$ has been calculated separately along each of the three normal vectors of the box defining the $\langle 1\,0\,0 \rangle$, $\langle 0\,1\,0 \rangle$ and $\langle 0\,0\,1 \rangle$ directions with $d$ taken as half of the lattice constant of the cubic unit cell. All three functions, one given in figure 13 (*a*) representatively, show the same behaviour within the statistical errors relating to the equivalence of the three orthogonal directions distinguished in a cubic blue phase. The modulation of the curves can be understood considering the network of the interwoven double twist cylinders identified in figure 7. The negative minimum at distances $r_\parallel^*/d = 1/4$ fits nicely with the existence of perpendicularly oriented double twist cylinders separated by a quarter of the lattice constant moving along one of the $\langle 1\,0\,0 \rangle$, $\langle 0\,1\,0 \rangle$ and $\langle 0\,0\,1 \rangle$ directions according to the body-centred cubic elementary cell of BP I, figure 6 (*a*); i.e. it is more likely that molecules separated by this distance are oriented perpendicular to each other. Additionally, the positive maximum at distances $r_\parallel^*/d = 1/2$ corresponds to the existence of parallel oriented double twist cylinders inside the unit cell separated by half of the lattice constant along the chosen reference axis, i.e. molecules separated by this distance have a higher probability of being parallel to each other. The very small quantities, especially compared with $S_{220}(r_\parallel^*/d)$ in the cholesteric phase, can be understood considering that only 29.45% of the space belong to orientationally correlated double twist cylinders in the theoretical model of BP I in the $O^{8-}$ structure [12]. For comparison, $S_{220}(r_\parallel^*/d)$ has been

additionally calculated for a blue phase II, obtained in a system of $N = 256$ molecules at $c^* = 1.1$ [26], again separately along each of the three normal vectors of the box defining the $\langle 1\,0\,0 \rangle$, $\langle 0\,1\,0 \rangle$ and $\langle 0\,0\,1 \rangle$ directions with $d$ as half of the lattice constant of the cubic unit cell. As in BP I, all three functions, one given in figure 13 (*a*) representatively, show the same behaviour within the statistical errors relating to the equivalence of the three orthogonal directions distinguished in a cubic blue phase. In comparison with $S_{220}(r_\parallel^*/d)$ calculated for blue phase I, a completely different behaviour is obvious both qualitatively and quantitatively. It varies monotonously from its positive maximum value for molecules separated by small values of $r_\parallel^*/d$ to its negative minimum value for molecules separated by a distance $r_\parallel^*/d = 1/2$. This fits well with the existence of perpendicularly oriented double twist cylinders separated by a half of the lattice constant according to the simple cubic elementary cell of BP II shown in figure 6 (*c*). No further positive maximum appears, corresponding to the lack of parallel oriented double twist cylinders inside the unit cell. The enlarged quantities, compared with $S_{220}(r_\parallel^*/d)$ in blue phase I, can be understood considering that now 58.9% of the space belongs to orientationally correlated double twist cylinders [12]. In the phase at $c^* = 2.0$, where no lattice structure of double twist cylinders was obvious in figure 9, $S_{220}(r_\parallel^*/d)$ calculated separately along each of the three box face normals with $d$ equal to the box size $L$, is zero for all distances, giving a further hint that the existing local double twist structures (proved especially by the large negative values of $S_{221}(r^*)$ and $S_{441}(r^*)$, figure 12, at small $r^*$), could be randomly arranged, as in the so-called spaghetti or double twist model of blue phase III.

All findings on the basis of $S_{220}(r_\parallel^*/d)$ are further confirmed considering the pseudoscalar longitudinal orientational correlation function $S_{221}(r_\parallel^*/d)$, figure 13 (*b*), calculated with respect to the corresponding reference axes and appropriately scaled. In the cholesteric phase, $S_{221}(r_\parallel^*/d)$ for instance is zero for molecules separated by $r_\parallel^*/d = 1/4$, i.e. for molecules separated by distances of $p/4$ along the helical axis, where on average the molecules are perpendicular to each other and no preferred handedness can be distinguished. Again, in all blue phases the functions $S_{221}(r_\parallel^*/d)$ calculated separately along each of the three normal vectors of the box are identical within the statistical errors. While in the phase at $c^* = 2.0$ $S_{221}(r_\parallel^*/d)$ is again zero for all distances, in the other blue phases the minima, at $r_\parallel^*/d = 1/8$ in blue phase I and at $r_\parallel^*/d = 1/4$ in blue phase II, correspond to the radius of the double twist cylinders, given by 1/8 and 1/4 of the unit cell length, respectively, where according to the theoretical models a twist of 45° relative to the centre of the cylinder should exist. Again, the significantly enlarged value of $S_{221}(r_\parallel^*/d)$ in the minimum for BP II corresponds to the higher amount of space filling by double twist regions compared with BP I.

## 6. Conclusions

A system of $N = 2048$ uniaxial chiral calamitic molecules with both translational and orientational degrees of freedom was investigated using Monte Carlo simulations in the $NVT$ ensemble. The anisotropic interactions between the chiral molecules were chosen as given for the chiral Gay–Berne fluid. A rich polymorphism of chiral liquid crystal phases, all characterized by order parameters, scalar and pseudoscalar orientational correlation functions, and visual representations of selected configurations, was observed along an isotherm with increasing chirality parameter describing the strength of the chiral interaction. In addition to the cholesteric phase (N*), for the first time by computer simulation of a many-particle system basing on model intermolecular interactions, a blue phase I (BP I) with the corresponding network of interwoven double twist cylinders could be proven. Additionally, at high values of the chirality parameter, a phase with randomly oriented squirming double twist tubes, the characteristics of the so-called spaghetti or double twist model for blue phase III (BP III), was found. The phase sequence nematic, cholesteric, blue phase I and a blue phase with randomly oriented double twist regions obtained with increasing chirality parameter, corresponds well to many experimentally observed phase diagrams which often show these universal features. At the same time, the phase diagram in the temperature–chirality parameter plane is no longer dominated by blue phase II (BP II), one of the findings in a previous study of a much smaller chiral Gay–Berne system [26], a phenomenon also obvious in many phase diagrams determined theoretically by means of Landau–de Gennes theory [12, 13]. Further investigations are necessary with respect to the absence of BP II along the studied isotherm. A future task is especially to determine whether the system shows a phase transition from BP I to BP II with increasing temperature. In a selected chirality parameter range, such a behaviour is often a characteristic feature of chiral liquid crystals, see e.g. the phase diagram in the temperature–chirality parameter plane sketched in figure 5 (*a*), i.e. the temperature studied could have been below the range of existence of BP II. A further possibility for the absence of BP II in the current simulation could be that the system has not been studied at appropriate values of $c^*$, especially as it is well known from experiments that BP II often exists only over a very narrow range of the chirality parameter along an isotherm. In general, the clear evidence should be emphasized that a chiral interaction potential proportional to the first pseudoscalar term of the expansion

in rotational invariants, $[(\hat{\mathbf{u}}_i \times \hat{\mathbf{u}}_j)\ \hat{\mathbf{r}}_{ij}](\hat{\mathbf{u}}_i\ \hat{\mathbf{u}}_j)$, is able to give both cholesteric and blue phases on variation of one pseudoscalar chirality parameter only. The restrictions caused by the small system size and the periodic boundary conditions, in the case of phases with periodic structures the situation corresponding closely to a study of confined systems, have to be kept in mind, especially with respect to the regions of existence of the different phases in the temperature–chirality parameter plane of the phase diagram, which might be strongly influenced by the formation of cholesteric and blue phases with non-equilibrium pitch and lattice constants, respectively. A future task is especially to overcome these restrictions. With respect to the cholesteric phase, simulations in the *NpT* which additionally allow the determination of the phase transition enthalpy and the heat capacity at constant pressure—especially interesting at high values of the chirality parameter with regard to the nature of the blue phase III–isotropic critical point [42, 48]—should enable the study of the equilibrium pitch and its temperature dependence. Of further interest is a more detailed characterization of the observed blue phases, both with respect to their dynamical properties and the structure of the disclinations [49].



Generous allocation of computer time by the Regionales Hochschulrechenzentrum Kaiserslautern and the John von Neumann-Institut für Computing, Jülich and financial support from the Deutsche Forschungsgemeinschaft and the Fonds der Chemischen Industrie are gratefully acknowledged.

## References

[1] Goodby, J. W., 1998, in *Handbook of Liquid Crystals*, edited by D. Demus, J. Goodby, G. W. Gray, H.-W. Spiess, and V. Vill (Weinheim: Wiley-VCH), pp. 115–132.
[2] Kuball, H.-G., Memmer, R., and Türk, O., 2000, in *Chiral Liquid Crystals*, edited by L. Komitov (Singapore: World Scientific Press) (in the press).
[3] Hauser, A., Thieme, M., Saupe, A., Heppke, G., and Krüerke, D., 1997, *J. mater. Chem.*, **7,** 2223.
[4] Li, M.-H., Laux, V., Nguyen, H.-T., Sigaud, G., Barois, P., and Isaert, N., 1997, *Liq. Cryst.*, **23,** 389.
[5] Spada, G. P., and Proni, G., 1998, *Enantiomer*, **3,** 301.
[6] Van Nostrum, C. F., Bosman, A. W., Gelinck, G. H., Schouten, P. G., Warman, J. M., Kentgens, A. P. M., Devillers, M. A. C., Meijerink, A., Picken, S. J., Sohling, U., Schouten, A.-J., and Nolte, R. J. M., 1995, *Chem. Eur. J.*, **1,** 171.
[7] Goodby, J. W., 1999, in *Liquid Crystals II*, edited by D. M. P. Mingos (Berlin: Springer), pp. 83–147.
[8] Pansu, B., Li, M. L., and Nguyen, H. T., 1998, *Eur. Phys. J. B*, **2,** 143.
[9] Lubensky, T. C., Harris, A. B., Kamien, R. D., and Yan, G., 1998, *Ferroelectrics*, **212,** 1.
[10] Ferrarini, A., Gottarelli, G., Nordio, P. L., and Spada, G. P., 1999, *J. chem. Soc., Perkin Trans. 2*, 411.
[11] Dubois-Violette, E., and Pansu, B., 1988, *Mol. Cryst. liq. Cryst.*, **165,** 151.
[12] Wright, D. C., and Mermin, N. D., 1989, *Rev. mod. Phys.*, **61,** 395.
[13] Seideman, T., 1990, *Rep. Prog. Phys.*, **53,** 659.
[14] Collings, P. C., 1997, *Mol. Cryst. liq. Cryst.*, **292,** 155.
[15] Allen, M. P., and Tildesley, D. J., 1987, *Computer Simulation of Liquids* (Oxford: Clarendon Press).
[16] Frenkel, D., and Smit, B., 1996, *Understanding Molecular Simulation* (San Diego: Academic Press).
[17] Pelcovits, R. A., 1997, in *Handbook of Liquid Crystal Research*, edited by P. J. Collings and J. S. Patel (Oxford: University Press), pp. 71–98.
[18] Pasini, P., and Zannoni, C. (editors), 1999, *Advances in the Computer Simulations of Liquid Crystals* (Dordrecht: Kluwer Academic Publishers).
[19] Bates, M. A., and Luckhurst, G. R., 1999, in *Liquid Crystals I*, edited by D. M. P. Mingos (Berlin: Springer), pp. 65–137.
[20] Tsykalo, A. L., 1979, *Zh. fiz. Khim.*, **53,** 2528 (1979, *Russ. J. phys. Chem.*, **53,** 1443).
[21] Memmer, R., Kuball, H.-G., and Schönhofer, A., 1996, *Mol. Phys.*, **89,** 1633.
[22] Sarman, S., 1999, *J. chem. Phys.*, **110,** 12 218.
[23] Luckhurst, G. R., Romano, S., and Zewdie, H. B., 1996, *J. chem. Soc., Faraday Trans.*, **92,** 1781.
[24] Saha, J., and Saha, M., 1997, *Mol. Sim.*, **19,** 227.
[25] Memmer, R., and Janssen, F., 1998, *J. chem. Soc., Faraday Trans.*, **94,** 267.
[26] Memmer, R., Kuball, H.-G., and Schönhofer, A., 1993, *Liq. Cryst.*, **15,** 345.
[27] Memmer, R., 1998, *Ber. Bunsenges, phys. Chem.*, **102,** 1002.
[28] Yang, D. K., and Crooker, P. P., 1987, *Phys. Rev. A*, **35,** 4419.
[29] Englert, J., Longa, L., Stark, H., and Trebin, H.-R., 1998, *Phys. Rev. Lett.*, **81,** 7.
[30] Osipov, M. A., 1993, in *Liquid Crystalline and Mesomorphic Polymers*, edited by V. B. Shibaev and L. Lam (New York: Springer), pp. 1–25.
[31] Gay, J. G., and Berne, B. J., 1981, *J. chem. Phys.*, **74,** 3316.
[32] Van der Meer, B. W., Vertogen, G., Dekker, A. J., and Ypma, J. G. J., 1976, *J. chem. Phys.*, **65,** 3935.
[33] Luckhurst, G. R., Stephens, R. A., and Phippen, R. W., 1990, *Liq. Cryst.*, **8,** 451.
[34] Stone, A. J., 1978, *Mol. Phys.*, **36,** 241.
[35] Blinov, L. M., and Chigrinov, V. G., 1996, *Electrooptic Effects in Liquid Crystal Materials* (Berlin: Springer).
[36] Allen, M., 1995, in *Observation, Prediction and Simulation of Phase Transitions in Complex Fluids*, edited by M. Baus, L. F. Rull, and J.-P. Ryckaert (Dordrecht: Kluwer Academic Publishers), pp. 557–591.
[37] Stegemeyer, H., Kersting, H.-J., and Kuczynski, W., 1987, *Ber. Bunsenges, phys. Chem.*, **91,** 3.
[38] Memmer, R., 1999, in Proceedings of the 28th Freiburger Arbeitstagung Flüssigkristalle, 24–26 March, Freiburg, Germany.
[39] Saupe, A., 1969, *Mol. Cryst. liq. Cryst.*, **7,** 59.
[40] De Gennes, P. G., and Prost, J., 1993, *The Physics of Liquid Crystals* (Oxford: University Press).
[41] Leforestier, A., and Livolant, F., 1994, *Liq. Cryst.*, **17,** 651.
[42] Lubensky, T. C., and Stark, H., 1996, *Phys. Rev. E*, **53,** 1996.

[43] Collings, P. J., 1990, *Liquid Crystals—Nature's Delicate Phase of Matter* (Bristol: Adam Hilger).
[44] Crooker, P. P., and Kitzerow, H.-S., 1992, *Cond. Matter News*, **1,** 6.
[45] Hornreich, R. M., 1991, *Phys. Rev. Lett.*, **67,** 2155.
[46] Longa, L., Fink, W., and Trebin, H.-R., 1993, *Phys. Rev. E*, **48,** 2296.
[47] Englert, J., Longa, L., and Trebin, H.-R., 1996, *Liq. Cryst.*, **21,** 243.
[48] Anisimov, M. A., Agayan, V. A., and Collings, P. C., 1998, *Phys. Rev. E*, **57,** 582.
[49] Schöbel, G., and Memmer, R., 1999, in Proceedings of the Workshop *Molecular Dynamics on Parallel Computers*, 8–10 February, Jülich, Germany.